

A Least-Squares Multi-Step Koopman Operator for Model Predictive Control [★]

Liang Wu^{* a,b}, Wallace Gian Yion Tan^{* b}, Leqi Zhou^b, Richard D. Braatz^b,
Jan Drgona^a

^a Johns Hopkins University, MD 21218, USA.

^b Massachusetts Institute of Technology, MA 02139, USA.

Abstract

MPC is widely used in real-time applications, but practical implementations are typically restricted to convex QP formulations to ensure fast and certified execution. Koopman-based MPC enables QP-based control of nonlinear systems by lifting the dynamics to a higher-dimensional linear representation. However, existing approaches rely on single-step EDMD. Consequently, prediction errors may accumulate over long horizons when the EDMD operator is applied recursively. Moreover, the multi-step prediction loss is nonconvex with respect to the single-step EDMD operator, making long-horizon model identification particularly challenging. This paper proposes a multi-step EDMD framework that directly learns the condensed multi-step state-control mapping required for Koopman-MPC, thereby bypassing explicit identification of the lifted system matrices and subsequent model condensation. The resulting identification problem admits a convex least-squares formulation. We further show that the problem decomposes across prediction horizons and state coordinates, enabling parallel computation and row-wise ℓ_1 -regularization for automatic dictionary pruning. A non-asymptotic finite-sample analysis demonstrates that, unlike one-step EDMD, the proposed method avoids error compounding and yields error bounds that depend only on the target multi-step mapping. Numerical examples validate improved long-horizon prediction accuracy and closed-loop performance.

Key words: Koopman Operator; Model Predictive Control; Extended Dynamic Mode Decomposition.

1 Introduction

Model predictive control (MPC) is a model-based optimal control framework that has been widely adopted in manufacturing, energy systems, and robotics. At each sampling instant, MPC requires the solution of a real-time online optimization problem defined by a prediction model, system constraints, and a performance objective. To enable reliable real-time execution, MPC is commonly formulated as a convex quadratic program

(QP), since QPs admit fast numerical solution methods [9,31,41] and allow execution-time-certified computation (ensuring that worst-case computation times satisfy real-time feedback constraints) [42,40,39] on industrial embedded platforms.

However, the standard QP formulation of MPC requires linear prediction dynamics, affine constraints, and a convex quadratic objective, which hinders its direct applicability in nonlinear dynamical systems. A common workaround to address this limitation is to approximate the nonlinear dynamics via online linearization about the current state or a previous solution trajectory, resulting in a sequence of QPs [3,10]. These methods are often referred to as model-based approximation approaches.

Recently, data-driven approximation approaches via the Koopman Operator have emerged as computationally efficient ways to handle nonlinear systems in QP-based MPC. By learning a surrogate linear dynamical system in a high-dimensional observable space, these Koopman-based methods enable nonlinear MPC problems to be

[★] Wallace Tan is supported by the MathWorks Fellowship. Liang Wu and Richard Braatz were partially supported by the U.S. Food and Drug Administration under the FDA BAA-22-00123 program, Award Number 75F40122C00200. This research was also supported by the Ralph O'Connor Sustainable Energy Institute at Johns Hopkins University. This paper was not presented at any IFAC meeting.

^{*}Equal Contributions. Corresponding Author: Liang Wu.

Email addresses: wliang14@jh.edu (Liang Wu*), wtgy@mit.edu (Wallace Gian Yion Tan*), leqizhou@mit.edu (Leqi Zhou), braatz@mit.edu (Richard D. Braatz), jdronga1@jh.edu (Jan Drgona).

cast as compact QPs after eliminating the lifted states via model condensation [15,2,37,30,20].

In contrast to localized linearization methods, Koopman-MPC approaches [15] aim to construct a globally valid linear predictor in the lifted observable space. This distinction is also reflected in the resulting control laws: linearization-based MPC yields a QP parameterized directly by the current state $x(t)$, i.e., $u(t) = \text{QP}(x(t))$, whereas Koopman-MPC yields a QP parameterized in a high-dimensional observable space via a nonlinear lifting map $\phi(\cdot)$, i.e., $u(t) = \text{QP}(\phi(x(t)))$. This richer parameterization explains the improved closed-loop performance often observed in Koopman-MPC [15].

1.1 Related work

The most widely used identification method in Koopman-based MPC is Extended Dynamic Mode Decomposition (EDMD) [38], which first specifies a dictionary of nonlinear lifting observables $\phi(\cdot)$ *a priori* and then solves a convex least-squares problem to identify the linear state-space matrices $\{A, B, C\}$. EDMD offers scalable computation and algorithmic simplicity due to its reliance on least-squares estimation, but this comes at the cost of limited representation capacity and sensitivity to the choice of nonlinear observable dictionary. Moreover, its least-squares structure enables analytical bounds on model approximation errors in Koopman-MPC, which provides a tractable foundation for theoretical analysis [32,46,23,24].

In [19,45], deep neural network (DNN) based representations of the observables and the linear state-space matrices $\{A, B, C\}$ are jointly identified through a nonconvex learning problem. Within the DNN framework, the training objective can naturally be extended to a multi-step prediction loss [43]. Notably, minimizing this loss promotes high-fidelity multi-step prediction, which is essential in finite-horizon MPC. In contrast, single-step predictors tend to accumulate prediction error as the MPC horizon increases. This may lead to degradation of open-loop and closed-loop performance [33], especially when the spectral radius of the Koopman matrix A exceeds unity, in which case prediction errors are amplified [33,6,17].

However, extending existing EDMD approaches to a multi-step prediction minimization setting necessitates terms of the form $\{A^k, \dots, A\}$, which breaks the convexity of the original least-squares problem and results in a nonconvex optimization formulation; see [7,29,18,28,1,8]. Moreover, condensing a Koopman-MPC problem into a QP ultimately requires the multi-step state-control mapping:

$$(x_1, \dots, x_H) = \mathbf{E}\phi(x(t)) + \mathbf{F}(u_0, \dots, u_{H-1})$$

which is obtained by recursively propagating the lifted linear dynamics defined by $\{A, B, C\}$ over the horizon H , where the matrices $\{\mathbf{E}, \mathbf{F}\}$ are constructed from $\{A, B, C\}$ accordingly.

1.2 Contributions

Motivated by this observation, this paper proposes a multi-step EDMD algorithm that directly learns the matrices $\{\mathbf{E}, \mathbf{F}\}$ governing the multi-step state-control mapping, thereby bypassing the identification of $\{A, B, C\}$ and the subsequent construction of $\{\mathbf{E}, \mathbf{F}\}$ used in conventional Koopman-MPC approaches. As a result, our algorithm admits a convex least-squares formulation.

In addition, this paper shows that the proposed multi-step EDMD identification problem can be decomposed at a prediction horizon level and state coordinates level, enabling parallelized identification of $\{\mathbf{E}, \mathbf{F}\}$ and facilitating the incorporation of row-wise ℓ_1 regularization on \mathbf{E} for dictionary pruning. Dictionary pruning mitigates the difficulty of dictionary selection by automatically removing functions that are irrelevant to the system dynamics. Consequently, we obtain a least-squares-based multi-step EDMD algorithm with parallelization and integrated dictionary pruning.

Furthermore, we provide a non-asymptotic analysis of both one-step and multi-step EDMD under finite data regimes. For one-step EDMD, we show that model errors compound through repeated composition, potentially leading to error growth that is exponential in the prediction horizon. In contrast, the proposed multi-step EDMD yields error bounds that depend only on the target multi-step mapping, rather than on the accuracy of intermediate EDMD approximations. This distinction provides a principled explanation for the improved long-horizon prediction performance observed with the proposed multi-step EDMD approach.

1.3 Notations

Denote \mathbb{Z}^+ as the set of positive integers and $\mathbb{N} := \{0\} \cup \mathbb{Z}^+$ as the set of natural numbers. Given a matrix $P \in \mathbb{R}^{n \times n}$, $P \succeq 0$ (resp., $P \succ 0$) denotes that P is symmetric positive semi-definite (resp., symmetric positive definite). For a given subset $\mathcal{U} \subset \mathbb{R}^n$ of admissible control actions, denote $\ell(\mathcal{U})$ as the space of all admissible control sequences $\{u_i\}_{i=0}^\infty$. Given matrices A_1, A_2, \dots, A_m with $A_i \in \mathbb{R}^{n_i \times n_i}$, $\text{blkdiag}(A_1, \dots, A_m) \in \mathbb{R}^{(\sum_i n_i) \times (\sum_i n_i)}$ denotes the block-diagonal matrices with entries A_i on the main diagonal and zero matrices everywhere else. \otimes denotes the standard Kronecker product. Given vectors v_1, v_2, \dots, v_n , let $\text{vec}[v_1, \dots, v_n] := [v_1^\top, v_2^\top, \dots, v_n^\top]^\top$. Let $\mathbf{1}^n \in \mathbb{R}^n$ denote the vector with ones in all components. Denote $\|\cdot\|_2$ and $\|\cdot\|_1$ as the standard Euclidean

norm and ℓ^1 norms of v , respectively. For $n \in \mathbb{Z}^+$, let $[n] := \{0, 1, \dots, n\}$. If X and Y are Banach or Hilbert spaces and $A : X \rightarrow Y$ is a linear operator, $\mathcal{B}(X, Y)$ denotes the set of bounded linear operators between X and Y , and for $A \in \mathcal{B}(X, Y)$, $\|A\|_{X \rightarrow Y}$ denotes the operator norm of A . If $X = Y$, denote $\mathcal{B}(X, X)$ as $\mathcal{B}(X)$ and $\|A\|_X$ denotes the operator norm of A . If $A \in \mathbb{R}^{n \times m}$, denote $A^\dagger \in \mathbb{R}^{m \times n}$ as the Moore-Penrose inverse of A .

Throughout this article, ‘with high probability’ (w.h.p.) means with probability $1 - \delta$, where $\delta \in (0, 1)$ decays at least polynomially as the sample size increases. The dependence of δ on the sample size can be made explicit from the proofs.

2 Problem Formulation and Preliminaries

Consider the problem of regulating a nonlinear discrete-time system to the origin:

$$x_{t+1} = f(x_t, u_t), \quad (1)$$

where $x_t \in \mathbb{R}^{n_x}$ and $u_t \in \mathbb{R}^{n_u}$ denote the system state and control input at the sampling time $t \in \mathbb{Z}^+$. MPC addresses this problem by solving a finite-time optimal control problem subject to the dynamics in (1) and additional state and control input constraints. Assuming that a full measurement of the state $x(t)$ at the sampling time t is available, the finite horizon optimal control problem is shown in (2).

Nonlinear MPC

$$\min_U x_{t+H}^\top P x_{t+H} + \sum_{k=0}^{H-1} [x_{t+k}^\top Q x_{t+k} + u_{t+k}^\top R u_{t+k}] \quad (2a)$$

$$\text{s.t. } x_t = x(t), \quad (2b)$$

$$x_{t+k+1} = f(x_{t+k}, u_{t+k}), \quad k = 0, \dots, H-1 \quad (2c)$$

$$x_{\min} \leq x_{t+k+1} \leq x_{\max}, \quad k = 0, \dots, H-1 \quad (2d)$$

$$u_{\min} \leq u_{t+k} \leq u_{\max}, \quad k = 0, \dots, H-1 \quad (2e)$$

This optimization problem is solved at each sampling time t , where x_{t+k} denotes the predicted state vector at time $t + k$ obtained by applying the control input sequence u_t, \dots, u_{t+k-1} to the system (1) starting from the state $x(t)$, and H denotes the prediction horizon. In (2), we further assume that $Q = Q^\top \succeq 0$, $R = R^\top \succ 0$, $P = P^\top \succeq 0$. The decision variables in the optimization problem (2) are the control inputs $U := \{u_t, u_{t+1}, \dots, u_{t+H-1}\}$. The corresponding state trajectory $X := \{x_{t+1}, \dots, x_{t+H}\}$ is implicitly defined by the nonlinear system dynamics (2c) and the control input sequence U . The nonlinear MPC problem in general is a nonlinear program due to the nonlinear dynamics arising from (2c). Solving the nonlinear program at every

sampling time can be computationally expensive due to the general intractability of such problems, especially for the MPC problem with long prediction horizons. To mitigate the computational burden of this problem, the Koopman operator lifts the nonlinear systems (1) into a higher-dimensional space of observables, where the system evolves with linearized dynamics. This transformation allows the reformulation of (2) into a convex QP that can be solved using standard QP solvers such as interior point methods.

2.1 Koopman operator and Extended Dynamic Mode Decomposition

Koopman [14] proposed an approach grounded in operator theoretic methods to represent uncontrolled discrete-time nonlinear dynamical systems $x_{t+1} = f(x_t)$ linearly. Specifically, Koopman demonstrated the existence of an infinite-dimensional linear operator \mathcal{K} , which governs the evolution of an infinite-dimensional Hilbert space of observables. Given an observable function $\psi : \mathbb{R}^{n_x} \rightarrow \mathbb{R}$, the Koopman operator acts on ψ , and $\mathcal{K}\psi$ is defined as

$$\mathcal{K}\psi := \psi \circ f. \quad (3)$$

Although the Koopman operator was initially described for autonomous dynamical systems, numerous schemes (see [37, 26, 15, 32]) have been proposed to extend the application of the Koopman operator to controlled systems of the form (1). To generalize the Koopman operator to controlled systems, we adopt the scheme from [15] which

introduces an extended state vector: $\mathcal{X} = \begin{bmatrix} x \\ \mathbf{u} \end{bmatrix}$, where

$\mathbf{u} := \{\mathbf{u}(i)\}_{i=0}^\infty \in l(\mathcal{U})$. The dynamics of the extended state \mathcal{X} are described as $f_{\mathcal{X}}(\mathcal{X}) = \begin{bmatrix} f(x, \mathbf{u}(0)) \\ S\mathbf{u} \end{bmatrix}$, where

$\mathbf{u}(i)$ denotes the i th element of \mathbf{u} and S represents the left shift operator, $(S\mathbf{u})(i) := \mathbf{u}(i+1)$. Then, the Koopman operator associated with the dynamics of the extended state can be defined on the set of extended observables $\phi(\mathcal{X})$ as $\mathcal{K}\phi := \phi \circ f_{\mathcal{X}}$.

The infinite-dimensional Koopman operator must be truncated in practice, and several finite-dimensional approximations have been proposed (see, e.g., [38, 37, 15, 19, 11]). A widely utilized data-driven truncation method is (single-step) Extended Dynamic Mode Decomposition (EDMD), where the set of extended observables is defined as the ‘lifted’ mapping

$$\phi(x, \mathbf{u}) = \begin{bmatrix} \psi(x) \\ \mathbf{u}(0) \end{bmatrix}, \quad (4)$$

where $\psi(x) := [\psi_1(x), \dots, \psi_N(x)]^\top$, N is the number of observables (with $N \gg n_x$), and $\mathbf{u}(0)$ denotes the

first component of the sequence \mathbf{u} . The EDMD framework represents nonlinear observables $\phi(x, \mathbf{u})$ using a predefined basis function set (e.g., Radial basis functions used in [15], Koopman eigenfunctions in [21]) rather than learning the observables from data. Only the Koopman operator is learned via an optimization procedure. In particular, the approximate Koopman operator identification problem is reduced to a least-squares problem, which assumes that the sampled data $\{(x_j, \mathbf{u}_j), (x_{j,+}, \mathbf{u}_{j,+})\} \forall j = 1, \dots, M$ is collected with

the update mapping $\begin{bmatrix} x_{j,+} \\ \mathbf{u}_{j,+} \end{bmatrix} = \begin{bmatrix} f(x_j, \mathbf{u}_j(0)) \\ S\mathbf{u}_j \end{bmatrix}$, where

the subscript $+$ denotes the value at the next time step. An approximation of the Koopman operator, \mathcal{A} , is then obtained by solving

$$J(\mathcal{A}) = \min_{\mathcal{A}} \sum_{j=1}^M \|\phi(x_{j,+}, \mathbf{u}_{j,+}) - \mathcal{A}\phi(x_j, \mathbf{u}_j)\|^2. \quad (5)$$

Since there is no need to predict the rest of the control input sequence, the last n_u rows of \mathcal{A} can be discarded. Additionally, if we define $\bar{\mathcal{A}}$ as the remaining part of \mathcal{A} after discarding the part associated with the future control input, we observe that $\bar{\mathcal{A}}$ can be decomposed into $A \in \mathbb{R}^{N \times N}$ and $B \in \mathbb{R}^{N \times n_u}$ as $\bar{\mathcal{A}} = [A, B]$, so that the problem (5) can be reduced to

$$J(A, B) = \min_{A, B} \sum_{j=1}^M \|\psi(x_{j,+}) - A\psi(x_j) - B\mathbf{u}_j(0)\|_2^2. \quad (6)$$

According to [15], if the designed lifted mapping $\psi(x)$ contains the state x after the re-ordering $\psi(x) \leftarrow [x^\top, \psi(x)]^\top$, then the output matrix $C = [I, 0]$. The learned linear Koopman predictor model is given as

$$\psi_{k+1} = A\psi_k + Bu_k, \quad x_{k+1} = C\psi_{k+1}, \quad (7)$$

where $\psi_k := \psi(x_k) \in \mathbb{R}^{n_\psi}$ denotes the lifted state space and with $\psi_0 = \psi(x(t))$.

2.2 Condensed Koopman-MPC formulation

Although the Koopman operator may require a large lifted dimension to obtain an accurate linear approximation, this does not increase the dimension of the resulting QP problem. Specifically, by recursively applying (7) to eliminate the lifted states ψ_k , we obtain

$$\begin{bmatrix} x_{t+1} \\ x_{t+2} \\ \vdots \\ x_{t+H} \end{bmatrix} = \mathbf{E}\psi(x_t) + \mathbf{F} \begin{bmatrix} u_t \\ u_{t+1} \\ \vdots \\ u_{t+H-1} \end{bmatrix} \quad (8)$$

where

$$\mathbf{E} := \begin{bmatrix} CA \\ CA^2 \\ \vdots \\ CA^H \end{bmatrix}, \quad \mathbf{F} := \begin{bmatrix} CB & 0 & \cdots & 0 \\ CAB & CB & \cdots & 0 \\ \vdots & \vdots & \ddots & \vdots \\ CA^{H-1}B & CA^{H-2}B & \cdots & CB \end{bmatrix} \quad (9)$$

where H is the prediction horizon. By embedding (8) into the quadratic objective (2a) and the state constraint (2d), the nonlinear MPC (2) can be reduced to the condensed QP problem in the decision vector U shown in (10) [27]. The higher-dimensional observable $\psi(x_t)$ is computed only once per QP problem, and will not be performed in QP iterations. By performing the condensing procedure described above, the computational burden of having a high-dimensional Koopman lifting is substantially minimized when solving the MPC problem.

Condensed Koopman-MPC \rightarrow General QP

$$\min_U U^\top \bar{R} U + (\mathbf{E}\psi(x_t) + \mathbf{F}U)^\top \bar{Q} (\mathbf{E}\psi(x_t) + \mathbf{F}U) \quad (10a)$$

$$\text{s.t. } \mathbf{1}^H \otimes x_{\min} \leq \mathbf{E}\psi(x_t) + \mathbf{F}U \leq \mathbf{1}^H \otimes x_{\max} \quad (10b)$$

$$\mathbf{1}^H \otimes u_{\min} \leq U \leq \mathbf{1}^H \otimes u_{\max} \quad (10c)$$

where $\bar{R} = \text{blkdiag}(R, \dots, R)$ and $\bar{Q} = \text{blkdiag}(Q, \dots, Q, P)$.

3 Multi-step Extended Dynamic Mode Decomposition

Data-driven Koopman operators inevitably introduce approximation errors, and the key to successfully integrating Koopman operators with MPC is ensuring that these approximation errors do not accumulate along the prediction horizon. However, the EDMD approach in Subsection 2.1, particularly (6), is based on minimizing one-step-ahead prediction error, and could potentially suffer from accumulated approximation errors, especially in scenarios with a long prediction horizon. Consequently, the one-step-ahead EDMD approach (6) can be modified to incorporate multi-step prediction error:

$$\min_{A, B} \sum_{j=1}^{M_m} \sum_{k=1}^H \left\| \psi(x_{j,k}) - A^k \psi(x_{j,0}) - \sum_{m=0}^{k-1} A^{k-1-m} B u_{j,m} \right\|_2^2, \quad (11)$$

where H is the prediction horizon and M_m is the number of sampling data trajectories:

$$\mathcal{D} = \{(x_{j,k}, x_{j,0}, u_{j,k-1})\}, \quad \forall j \in [1, M_m], \quad \forall k \in [1, H]$$

($x_{j,k}$ and $u_{j,k}$ denote the state and control input at the k th sampling time of the j th trajectory). However, (11)

is neither a convex nor a least-squares optimization problem, as compared to (6).

This article proposes a least-squares-based multi-step EDMD approach for real-time MPC applications. Inspired by the observation that the Koopman-MPC framework ultimately uses the representation (8) (the matrices \mathbf{E} and \mathbf{F}), rather than the intermediate matrices A and B , our proposed multi-step EDMD approach directly learns the matrices \mathbf{E} and \mathbf{F} in (8) from the data \mathcal{D} . Specifically, we obtain \mathbf{E} and \mathbf{F} from the multi-step prediction error minimization problem:

$$\min_{\mathbf{E}, \mathbf{F}} \sum_{j=1}^{M_m} \left\| X_j - \mathbf{E}\psi(x_{j,0}) - \mathbf{F}U_j \right\|_2^2 \quad (12)$$

where $X_j = \text{vec}[x_{j,1}, x_{j,2}, \dots, x_{j,H}]$ and $U_j = \text{vec}[u_{j,0}, u_{j,1}, \dots, u_{j,H-1}]$ are trajectory samples from the data set \mathcal{D} . This reformulated problem is now a least-squares optimization that is convex and further parallelizable.

Remark 1 (Representation power of multi-step EDMD): In conventional one-step EDMD, a linear-time-invariant model

$$\begin{aligned} \psi_{k+1} &= A\psi_k + Bu_k \\ x_k &= C\psi_k \end{aligned}$$

is learned to approximate the nonlinear dynamics. Our proposed multi-step EDMD approach directly learns the condensed MPC matrices \mathbf{E} and \mathbf{F} , which can implicitly encode the dynamics as linear horizon-varying models of the form

$$\begin{aligned} \psi_{k+1} &= A_k\psi_k + B_ku_k, \quad k = 0, \dots, H-1, \\ x_{k+1} &= C_k\psi_{k+1}, \quad k = 0, \dots, H-1. \end{aligned} \quad (13)$$

Thus, our approach has better representation power as compared to the conventional one-step EDMD.

3.1 Decomposition at the prediction horizons level and state coordinates level

To enforce the structural constraint that \mathbf{F} is a lower triangular matrix, this article adopts a simple trick that learns E_k, F_k , namely the k -th row-block of \mathbf{E} and \mathbf{F} defined in (12) that approximates x_k by right multiplication with $\psi(x_0)$ and u_0, \dots, u_{k-1} , independently and in parallel. To do so, we divide the whole dataset \mathcal{D} into H pieces, each of which corresponds to one horizon step $k \in [1, H]$. For $k = 1, \dots, H$, denote

$$\mathcal{D}_k = \{(x_{j,k}, x_{j,0}, u_{j,0}, \dots, u_{j,k-1})\}_{j=1}^{M_m}.$$

We can then solve the least-squares optimization problems in parallel:

for $k = 1 : H$ (**in parallel**)

$$\min_{E_k, F_k} \sum_{\mathcal{D}_k} \left\| x_{j,k} - E_k\psi(x_{j,0}) - F_k \begin{bmatrix} u_{j,0} \\ \vdots \\ u_{j,k-1} \end{bmatrix} \right\|_2^2 \quad (14)$$

end

Remark 2 Due to the parallel property of matrix-vector multiplication, (14) can be equivalently decomposed into the parallelizable subproblems

for $i = 1 : n_x$, $k = 1 : H$ (**in parallel**)

$$\min_{E_{k,i}, F_{k,i}} \sum_{\mathcal{D}_k} \left\| x_{j,k}^i - E_{k,i}^\top \psi(x_{j,0}) - F_{k,i}^\top \begin{bmatrix} u_{j,0} \\ \vdots \\ u_{j,k-1} \end{bmatrix} \right\|_2^2$$

end

where $x_{j,k}^i$ denotes the i th element of $x_{j,k}$, $E_{k,i}$ and $F_{k,i}$ denote the transposes of i th row vectors of matrices E_k and F_k , respectively.

4 Theoretical Analysis

This section provides a comparative analysis of the learning error of conventional single-step EDMD and multi-step EDMD for long-horizon prediction. In Section 2.1, we observed that single-step EDMD learns a single-step Koopman operator and generates long-horizon predictions by composing the linear predictor model. This single-step approach may potentially lead to the accumulation of approximation error across the prediction horizon in MPC. In contrast, our multi-step EDMD method in Section 3 learns the horizon-dependent input-output matrices, which directly circumvents the issue of error accumulation. To justify our hypothesis, we provide non-asymptotic error bounds under finite data budgets to demonstrate that multi-step EDMD yields stable long-horizon predictions. Our finite-sample analysis uses the Matrix Bernstein Inequality (Theorem 5.4.1 in [36]), which complements existing approaches in the EDMD literature [23, 46, 24, 25, 13].

4.1 Analysis framework and assumptions

We first begin with a framework for the analysis of both methods. We consider a discrete-time autonomous dynamical system $x_{t+1} = f(x_t)$, where Ω is a compact subset of \mathbb{R}^{n_x} and $f : \Omega \rightarrow \Omega$ is continuous. For concreteness, we take $\Omega = [-1, 1]^{n_x}$ equipped with the uniform probability measure $d\mu = 2^{-n_x} dx$, which simplifies the analysis and allows for canonical choices of observables such

as Polynomial Chaos Expansions (PCEs). This choice is not essential to the results presented in this section.

The Koopman operator defined in (3) is a linear operator that acts on an infinite-dimensional vector space of observable functions, and therefore its analysis requires a suitable function space. Let $\mathcal{H} = L^2(\mu)$ be the Hilbert space of square-integrable functions with respect to μ , equipped with the inner product

$$\langle f, g \rangle_{\mathcal{H}} := \int_{\Omega} f g \, d\mu = \frac{1}{2^{n_x}} \int_{[-1,1]^{n_x}} f g \, dx. \quad (16)$$

Remark 3 *The Hilbert space norm admits the probabilistic representation:*

$$\|f\|_{\mathcal{H}}^2 = \int_{\Omega} f^2 \, d\mu = \mathbb{E}_{x \sim \mu} [f(x)^2]. \quad (17)$$

To avoid notational clutter, we consistently use the Hilbert space norm with the understanding that $\|f\|_{\mathcal{H}}^2 = \mathbb{E}_{x \sim \mu} [f^2]$.

Throughout the article, we assume that the Koopman operator is always bounded to allow repeated composition.

Assumption 1 *The Koopman operator $\mathcal{K} \in \mathcal{B}(\mathcal{H})$ is a bounded linear operator on \mathcal{H} .*

Assumption 1 holds whenever $\mu \circ f^{-1} \ll \mu$ is absolutely continuous, and the Radon-Nikodym derivative $\frac{d\mu \circ f^{-1}}{d\mu}$ is bounded. Indeed, for any $\psi \in L^2(\mu)$,

$$\begin{aligned} \|\psi \circ f\|_{\mathcal{H}}^2 &= \int_{\Omega} (\psi \circ f)^2 \, d\mu = \int_{\Omega} \psi^2 \, d(\mu \circ f^{-1}) \\ &\leq \left\| \frac{d\mu \circ f^{-1}}{d\mu} \right\|_{L^{\infty}(\mu)} \|\psi\|_{\mathcal{H}}^2. \end{aligned} \quad (18)$$

Thus \mathcal{K} is a bounded linear operator.

4.2 Koopman approximations for EDMD

4.2.0.1 Single-step EDMD We first review some operator-theoretic properties of the conventional single-step Koopman operator and EDMD approximations. Approximating the Koopman operator \mathcal{K} numerically requires restriction to a finite-dimensional vector space of observables. Specifically, let $\{\psi_l\}_{l=1}^{\infty}$ be a complete orthonormal basis of observables in \mathcal{H} , and let $\mathcal{F}_N := \text{span}\{\psi_l\}_{l=1}^N$ be the dictionary. The projection of the Koopman operator onto \mathcal{F}_N is

$$\mathcal{K}_N := P_N \mathcal{K} \big|_{\mathcal{F}_N}, \quad (19)$$

where P_N denotes the Hilbert space projection onto the subspace \mathcal{F}_N . When \mathcal{K}_N is viewed as an operator on \mathcal{H} , we implicitly identify \mathcal{K}_N with its natural extension $P_N \mathcal{K} P_N$.

We now recollect some important properties of \mathcal{K}_N . Since $P_N \rightarrow I$ strongly and \mathcal{K} is a bounded linear operator, $\mathcal{K}_N \rightarrow \mathcal{K}$ in the strong operator topology. This means that, for any $g \in \mathcal{H}$,

$$\lim_{N \rightarrow \infty} \|\mathcal{K}_N g - \mathcal{K} g\|_{\mathcal{H}} = 0. \quad (20)$$

The details can be found in Thm. 3 of [16]. Additionally, for any $g \in \mathcal{F}_N$,

$$\mathcal{K}_N g = \arg \min_{h \in \mathcal{F}_N} \|\mathcal{K} g - h\|. \quad (21)$$

In single-step EDMD, we are given i.i.d samples $\{x_j\}_{j=1}^M \sim \mu$ and consider the empirical measure $\hat{\mu}_M := \sum_{j=1}^M \delta_{x_j}$ where δ_x is the Dirac delta measure at x . This equips \mathcal{H} with the empirical inner product

$$\langle f, g \rangle_M := \frac{1}{M} \sum_{j=1}^M f(x_j) g(x_j), \quad (22)$$

and we denote $P_{N,M} : \mathcal{H} \rightarrow \mathcal{F}_N$ as the orthogonal projection with respect to $\hat{\mu}_M$. Similarly, define the EDMD operator as

$$\mathcal{K}_{N,M} := P_{N,M} \mathcal{K} \big|_{\mathcal{F}_N}, \quad (23)$$

and identify $\mathcal{K}_{N,M}$ with its implicitly defined natural extension $P_{N,M} \mathcal{K} P_N$ on \mathcal{H} . Since \mathcal{F}_N is finite dimensional, the almost sure convergence of $\mathcal{K}_{N,M} g \rightarrow \mathcal{K}_N g$ for any $g \in \mathcal{F}_N$ implies that $\mathcal{K}_{N,M} \rightarrow \mathcal{K}_N$ almost surely in the operator norm topology,

$$\lim_{M \rightarrow \infty} \|\mathcal{K}_{N,M} - \mathcal{K}_N\|_{\mathcal{F}_N} = 0. \quad (24)$$

Let $\psi(x) := [\psi_1(x), \dots, \psi_N(x)]^\top$ be the vector with observable entries from \mathcal{F}_N . The single-step EDMD constructs the approximation $\mathcal{K}_{N,M} : \mathcal{F}_N \rightarrow \mathcal{F}_N$ by solving the empirical loss problem

$$A_{N,M} = \arg \min_{A \in \mathbb{R}^{N \times N}} \frac{1}{M} \sum_{j=1}^M \|\psi(f(x_j)) - A\psi(x_j)\|_2^2 \quad (25)$$

where $A_{N,M}$ is the matrix representation of $\mathcal{K}_{N,M}$ on the basis \mathcal{F}_N . If we define

$$\mathbf{G}_M := \frac{1}{M} \sum_{j=1}^M \psi(x_j) \psi(x_j)^\top, \quad \mathbf{A}_M := \frac{1}{M} \sum_{j=1}^M \psi(f(x_j)) \psi(x_j)^\top \quad (26)$$

then a solution to the empirical loss problem (25) is

$$A_{N,M} = \mathbf{G}_M^\dagger \mathbf{A}_M. \quad (27)$$

Once $A_{N,M}$ is computed, it can be used to generate predictions of the dynamics. For simplicity, we first impose an assumption that is true for many choices of observables, such as polynomial dictionaries.

Assumption 2 For any $i \in [1, n_x]$, the coordinate observables $g_i : \Omega \rightarrow \mathbb{R}$ defined by $g_i(x) := x^i$, where x^i is the i th coordinate of x , satisfy $g_i \in \mathcal{F}_N$.

Specifically, this assumption implies that, for any $g \in \mathcal{F}_N$, there exists a unique coefficient vector $a_g \in \mathbb{R}^N$ such that $g = a_g^\top \psi$. We then define the output matrix $C \in \mathbb{R}^{n_x \times N}$ by

$$C := [a_{g_1}, \dots, a_{g_{n_x}}]^\top$$

and a corresponding output operator $\mathcal{C} : \mathcal{F}_N \rightarrow \mathbb{R}^{n_x}$ by $\mathcal{C}g := Ca_g$. Given a current state $x_0 \in \Omega$, we first lift it into the observable space $z_0 = \psi(x_0)$, and evolve the dynamics linearly in the observable space by iterating $z_{i+1} \approx A_{N,M} z_i$. Thus, we have the approximate linear-time invariant (LTI) dynamics

$$z_t = A_{N,M} z_{t-1}, \quad (28a)$$

$$x_t = C z_t. \quad (28b)$$

4.2.0.2 Polynomial chaos expansions as dictionary observables Up to now, the Koopman operator framework is agnostic with respect to the choice of the complete orthonormal basis of observables $\{\psi_l\}_{l=1}^\infty$. To obtain explicit non-asymptotic error bounds for the bias error between \mathcal{K} and \mathcal{K}_N , we adopt a concrete choice of observables by using polynomial chaos expansions, which are the canonical choice for the uniform measure on Ω . The (normalized) Legendre polynomials $\{\Phi_\alpha(x)\}_{\alpha \in \mathbb{N}}$ form a complete orthonormal basis of $L^2([-1, 1])$ and are given by the formula:

$$\phi_\ell(x) = \sqrt{2\alpha + 1} \frac{1}{2^\alpha \alpha!} \frac{d^\alpha}{dx^\alpha} [(x^2 - 1)^\alpha] \quad (29)$$

Given a multi-index $\alpha = (\alpha_1, \alpha_2, \dots, \alpha_{n_x}) \in \mathbb{N}^{n_x}$, and $x = (x^1, x^2, \dots, x^{n_x}) \in \mathbb{R}^{n_x}$, define

$$\Phi_\alpha(x) := \prod_{i=1}^{n_x} \phi_{\alpha_i}(x^i). \quad (30)$$

It then follows that any $g \in \mathcal{H}$ can be written as a Polynomial Chaos Expansion (PCE):

$$g(x) = \sum_{\alpha \in \mathbb{N}^{n_x}} c_\alpha \Phi_\alpha(x). \quad (31)$$

Truncation of the series 31 enables us to approximate g as a PCE with some residual \mathcal{H} error. The following theorems provide a non-asymptotic bound of this projection error assuming the Sobolev regularity of g .

Lemma 1 For any $g \in H_\mu^s(\Omega)$, there exists a constant $C_{s,n_x} > 0$ only depending on $s > 0$ and n_x such that, for any $0 \leq q \leq \lfloor s/2 \rfloor$,

$$\left\| g - \sum_{\alpha \in [p]^{n_x}} c_\alpha \Phi_\alpha \right\|_{H_\mu^q(\Omega)} \leq C_{s,n_x} p^{e(q,s)} \|g\|_{H_\mu^s(\Omega)} \quad (32)$$

where

$$e(q,s) := \begin{cases} 2q - s - \frac{1}{2}, & q > 0 \\ -s, & q = 0 \end{cases} \quad (33)$$

and $\|g\|_{H_\mu^q(\Omega)}$ denotes the weighted Sobolev norm

$$\|g\|_{H_\mu^q(\Omega)} := \left(\sum_{\|\alpha\|_1 \leq q} \|D^\alpha g\|_{\mathcal{H}}^2 \right)^{1/2}. \quad (34)$$

Proof 1 The proof is found in Thms. 2.3 and 2.4 of [4].

By noting $H_\mu^0(\Omega) = \mathcal{H}$, the above theorem demonstrates that, by using the multivariate Legendre basis, the population approximation error for any $g \in H_\mu^s(\Omega)$ decays at a rate $O(p^{-s})$, where p is the maximal degree of the polynomial in each coordinate. This allows us to quantify the bias error for both single-step EDMD and multi-step EDMD, which will be utilized later. First, we make some assumptions on the discrete-time dynamics and the Koopman operator:

Assumption 3 (Regularity) For each $k \in [H]$, the k -step map $f^{(k)} : \Omega \rightarrow \Omega$ belongs to $H_\mu^s(\Omega)$ for some $s \geq 2$, i.e., it is weakly differentiable up to order s and $\|f^{(k)}\|_{H_\mu^s(\Omega)} < \infty$.

Remark 4 Since $f^{(k)} : \Omega \rightarrow \Omega \subseteq \mathbb{R}^{n_x}$ is vector-valued, we interpret the Sobolev norm component-wise, i.e.

$$\|f^{(k)}\|_{H_\mu^s(\Omega)}^2 := \sum_{i=1}^{n_x} \|f_i^{(k)}\|_{H_\mu^s(\Omega)}^2 \quad (35)$$

where $f_i^{(k)}$ is the i th component of $f^{(k)}$.

Assumption 4 (Koopman Regularity) $\mathcal{K} \in \mathcal{B}(H_\mu^s(\Omega))$ is a bounded linear operator on $H_\mu^s(\Omega)$ for some $s \geq 2$.

For all subsequent analyses, we choose as our dictionary the tensor product of Legendre polynomials with maximum degree p in each coordinate $\psi(x) := \{\Phi_\alpha(x)\}_{\alpha \in [p]^{n_x}}$. Note that the dimension of ψ is $N = (p+1)^{n_x}$.

4.2.0.3 Regression lemma The estimation error in least-squares EDMD algorithms reduces to standard linear regression problems, as seen in (14) and (25). We state a high-probability regression below that will be used in the error analysis of both single-step and multi-step EDMD.

Lemma 2 (Regression Error) *Let $\{(\psi(x_j), y(x_j)\}_{j=1}^M$ be i.i.d. samples with $x_j \sim \mu$ and $|y(x_j)| \leq M_y$ almost surely. Assume*

$$\Sigma := \mathbb{E}[\psi(x)\psi(x)^\top] = I_N.$$

Define the population minimizer

$$\beta_* := \arg \min_{\beta \in \mathbb{R}^N} \|y - \beta^\top \psi\|_{\mathcal{H}}^2,$$

and the empirical quantities

$$\widehat{\Sigma} := \frac{1}{M} \sum_{j=1}^M \psi(x_j)\psi(x_j)^\top, \quad \widehat{g} := \frac{1}{M} \sum_{j=1}^M \psi(x_j)y(x_j),$$

with estimator $\widehat{\beta} := \widehat{\Sigma}^{-1}\widehat{g}$. Then, under the uniform norm bound in Lemma 3, with probability at least $1 - 2M^{-2}$,

$$\|y - \widehat{\beta}^\top \psi\|_{\mathcal{H}}^2 - \|y - \beta_*^\top \psi\|_{\mathcal{H}}^2 \leq C_l \frac{M_y^2 N^2 \log M}{M}, \quad (36)$$

for a universal constant $C_l > 0$.

Proof 2 The proof is deferred to Appendix A.

4.2.0.4 Single-step EDMD We now apply the results in Lemmas 1 and 2 to analyze the approximation error of conventional single-step EDMD. Specifically, combining the bounds in (32) and (36) yields the following high-probability bound:

Theorem 1 *Let $\mathcal{K}_{N,M}$ be the EDMD operator with its matrix representation satisfying (25). Define*

$$B_{f,N} := \max_{l \in [1,N]} \|P_N(\psi_l \circ f)\|_{L^\infty(\mu)}. \quad (37)$$

Then w.h.p., for any $g \in H_\mu^s(\Omega)$ and $0 < q \leq \lfloor s/2 \rfloor$,

$$\|\mathcal{K}g - \mathcal{K}_{N,M}g\|_{\mathcal{H}} \leq \text{Err}_{N,M}^{\text{ss}}(g), \quad (38)$$

where

$$\text{Err}_{N,M}^{\text{ss}}(g) := C_{\text{ss}} \left((p^{-s} \|\mathcal{K}\|_{\mathcal{H}} + p^{q-s-1/2} \|\mathcal{K}\|_{H_\mu^q(\Omega)}) \|g\|_{H_\mu^s(\Omega)} \right. \\ \left. + p^{-q} \|\mathcal{K}\|_{H_\mu^q(\Omega)} \|g\|_{H_\mu^q(\Omega)} \right) \quad (39)$$

$$+ \sqrt{\frac{B_{f,N}^2 N^3 \log M}{M}} \|g\|_{\mathcal{H}} \Big), \quad (40)$$

and $C_{\text{ss}} > 0$ is a constant depending only on $s > 0$ and n_x .

Proof 3 The proof is deferred to Appendix B. The argument is similar to the multi-step case with differing minor technical details.

Equipped with the error bound (40) for single-step EDMD, we can then analyze the L^2 error when the single-step EDMD operator is applied recursively to predict future states. Specifically, for any $g \in H_\mu^s(\Omega)$ and horizon step $k \in [1, H]$, we have the telescoping identity:

$$\|\mathcal{K}^k g - \mathcal{K}_{N,M}^k g\|_{\mathcal{H}} = \left\| \sum_{\ell=0}^{k-1} \mathcal{K}_{N,M}^\ell (\mathcal{K}_{N,M} - \mathcal{K}) \mathcal{K}^{k-1-\ell} g \right\|_{\mathcal{H}} \\ \leq \sum_{\ell=0}^{k-1} \|\mathcal{K}_{N,M}\|_{\mathcal{H}}^\ell \|(\mathcal{K}_{N,M} - \mathcal{K}) \mathcal{K}^{k-1-\ell} g\|_{\mathcal{H}}.$$

By the single-step EDMD error bound in Thm. 1, we have w.h.p.,

$$\|(\mathcal{K}_{N,M} - \mathcal{K}) \mathcal{K}^{k-1-\ell} g\|_{\mathcal{H}} \leq \text{Err}_{N,M}^{\text{ss}}(\mathcal{K}^{k-1-\ell} g). \quad (41)$$

Hence,

$$\|\mathcal{K}^k g - \mathcal{K}_{N,M}^k g\|_{\mathcal{H}} \leq \sum_{\ell=0}^{k-1} \|\mathcal{K}_{N,M}\|_{\mathcal{H}}^\ell \text{Err}_{N,M}^{\text{ss}}(\mathcal{K}^{k-1-\ell} g), \quad (42)$$

which yields the desired multi-step error decomposition for conventional single-step EDMD. Applying the multi-step error decomposition (42) to the coordinate observables $g_i(x) = x^i$, since $\mathcal{K}^k g_i = f_i^{(k)}(x)$ and $\mathcal{K}_{N,M}^k g_i = a_{g_i}^\top A_{N,M}^k \psi(x)$, we obtain

$$\|f_i^{(k)} - a_{g_i}^\top A_{N,M}^k \psi\|_{\mathcal{H}} \leq \sum_{\ell=0}^{k-1} \|\mathcal{K}_{N,M}\|_{\mathcal{H}}^\ell \text{Err}_{N,M}^{\text{ss}}(f_i^{(k-1-\ell)}). \quad (43)$$

This decomposition explicitly highlights the accumulation of error across the prediction horizon. Specifically, if $\|\mathcal{K}_{N,M}\|_{\mathcal{H}} = \|A_{N,M}\|_2 > 1$, the errors at earlier time steps $\text{Err}_{N,M}^{\text{ss}}(f_i^{(k-1-\ell)})$ are amplified by the factor $\|\mathcal{K}_{N,M}\|_{\mathcal{H}}^\ell$. This motivates the formulation of multi-step condensed EDMD over a finite prediction horizon.

4.2.0.5 Multi-step condensed EDMD We now extend the operator-theoretic approximation framework for single-step EDMD to multi-step EDMD. Rather than considering the Koopman operator \mathcal{K} itself, we consider a finite-horizon Koopman map that encodes the time evolution of a given observable $g \in \mathcal{H}$ over the entire prediction horizon. Specifically, we define a multi-step Koopman map $\mathcal{T}^H : \mathcal{H} \rightarrow \mathcal{H}^H$,

$$\mathcal{T}^H g := (\mathcal{K}g, \mathcal{K}^2g, \dots, \mathcal{K}^Hg). \quad (44)$$

Under Assumption 1, $\mathcal{T}^H \in \mathcal{B}(\mathcal{H}, \mathcal{H}^H)$ is a bounded linear operator, as the projection to each component is bounded and there are finitely many components. We define the block-diagonal projection operator $P_N^H : \mathcal{H}^H \rightarrow \mathcal{F}_N^H$ by direct-sum extension:

$$P_N^H := \text{diag}[\underbrace{P_N, P_N, \dots, P_N}_{H \text{ times}}]. \quad (45)$$

The projection of the multi-step Koopman map onto \mathcal{F}_N^H is

$$\mathcal{T}_N^H := P_N^H \mathcal{T}^H|_{\mathcal{F}_N}. \quad (46)$$

When \mathcal{T}_N^H is viewed as an operator on \mathcal{H} , we implicitly identify \mathcal{T}_N^H with its natural extension $P_N^H \mathcal{T} P_N$. Since $P_N^H \rightarrow I$ strongly and \mathcal{K} is a bounded linear operator, it follows that $\mathcal{T}_N^H \rightarrow \mathcal{T}^H$ in the strong operator topology. Additionally, for any $g \in \mathcal{F}_N$, we have the variational formulation

$$\mathcal{T}_N^H g = \arg \min_{h \in \mathcal{F}_N^H} \|\mathcal{T}^H g - h\|. \quad (47)$$

Define the multi-step output operator $\mathcal{C} : \mathcal{F}_N^H \rightarrow (\mathbb{R}^{n_x})^H$ by

$$\mathcal{C}^H := \text{diag}[\underbrace{\mathcal{C}, \mathcal{C}, \dots, \mathcal{C}}_{H \text{ times}}]. \quad (48)$$

The condensed multi-step Koopman operator $\mathcal{E}_N^H : \mathcal{F}_N \rightarrow (\mathbb{R}^{n_x})^H$ is then defined by

$$\mathcal{E}_N^H g := \mathcal{C}^H \mathcal{T}_N^H g = (\mathcal{C} P_N \mathcal{K} g, \dots, \mathcal{C} P_N \mathcal{K}^H g). \quad (49)$$

Analagous to the single-step EDMD case, we are given samples of trajectories $\{(x_{j,0}, X_j)\}_{j=0}^{M_m}$, where $x_{j,0}$ are i.i.d samples from μ and $X_j := [x_{j,1}, \dots, x_{j,H}]$ is obtained by applying the dynamics $x_{j,k+1} = f(x_{j,k})$. With the same empirical measure $\hat{\mu}_{M_m} := \sum_{j=1}^{M_m} \delta_{x_j}$ and empirical inner product defined in (22) with M_m samples, define the block-diagonal projection operator $P_{N,M_m}^H : \mathcal{H}^H \rightarrow \mathcal{F}_N^H$ by direct sum extension:

$$P_{N,M_m}^H := \text{diag}[\underbrace{P_{N,M_m}, \dots, P_{N,M_m}}_{H \text{ times}}]. \quad (50)$$

We can define the empirical multi-step EDMD operator analogously to

$$\mathcal{T}_{N,M_m} := P_{N,M_m}^H \mathcal{T}^H|_{\mathcal{F}_N}, \quad (51)$$

and identify \mathcal{T}_{N,M_m} with its implicitly defined natural extension $P_{N,M_m}^H \mathcal{T} P_N$ on \mathcal{H} . The condensed multi-step EDMD operator $\mathcal{E}_{N,M_m}^H : \mathcal{F}_N \rightarrow (\mathbb{R}^{n_x})^H$ is then defined as

$$\mathcal{E}_{N,M_m}^H g := \mathcal{C}^H \mathcal{T}_{N,M_m}^H g = (\mathcal{C} P_{N,M_m} \mathcal{K} g, \dots, \mathcal{C} P_{N,M_m} \mathcal{K}^H g) \quad (52)$$

Since \mathcal{F}_N is finite dimensional, the almost sure convergence of $\mathcal{T}_{N,M_m}^H g \rightarrow \mathcal{T}_N^H g$ for any $g \in \mathcal{F}_N$ as $M_m \rightarrow \infty$ implies that $\mathcal{E}_{N,M_m}^H \rightarrow \mathcal{E}_N^H$ almost surely in the operator norm topology:

$$\lim_{M_m \rightarrow \infty} \|\mathcal{E}_{N,M_m}^H - \mathcal{E}_N^H\|_{\mathcal{F}_N \rightarrow (\mathbb{R}^{n_x})^H} = 0. \quad (53)$$

With the same $\psi(x) = [\psi_1(x), \dots, \psi_N(x)]^\top$ vector with observable entries from \mathcal{F}_N , multi-step EDMD constructs the approximation \mathcal{E}_{N,M_m}^H by solving the multi-step empirical trajectory loss problem,

$$\mathbf{E}_{N,M_m} = \arg \min_{\mathbf{E} \in \mathbb{R}^{n_x H \times N}} \frac{1}{M_m} \sum_{j=1}^{M_m} \left\| X_j - \mathbf{E} \psi(x_{j,0}) \right\|_2^2, \quad (54)$$

where \mathbf{E}_{N,M_m} is the matrix representation of \mathcal{E}_{N,M_m}^H on the basis \mathcal{F}_N .

Remark 5 Reiterating Remark 2, we again emphasize that, due to the parallel property of matrix-vector multiplication, the EDMD trajectory loss problem in (54) can be decomposed into the parallelizable subproblems

for $i = 1 : n_x$, $k = 1 : H$ (**in parallel**)

$$\min_{E_{k,i}} \frac{1}{M_m} \sum_{j=1}^{M_m} \|x_{j,k}^i - E_{k,i}^\top \psi(x_{j,0})\|_2^2 \quad (55)$$

end

4.2.0.6 Error bound for multi-step condensed EDMD Following the same reasoning as the single-step case, the results in Lemmas 1 and 2 can be similarly applied to analyze the approximation error of multi-step EDMD and compare it with (40). In particular, combining the bounds in (32) and (36) yields the following high-probability bound:

Theorem 2 (Multi-step EDMD Error) Let $\mathbf{E}_{N,M_m} = [E_1^\top, \dots, E_H^\top]^\top$ be the multi-step EDMD matrix obtained from (54). Under Assumption 3, for each $i \in [1, n_x]$,

$k \in [1, H]$, w.h.p., the L^2 error of multi-step EDMD satisfies

$$\|f_i^{(k)} - E_{k,i}^\top \psi\|_{\mathcal{H}} \leq C_{\text{ms}} \left(p^{-s} \|f_i^{(k)}\|_{H_\mu^s(\Omega)} + \sqrt{\frac{N^2 \log M_m}{M_m}} \right) \quad (56)$$

where $C_{\text{ms}} > 0$ is a constant depending only on $s > 0$ and n_x .

Proof 4 Let $E_{k,i}^*$ denote the parameter that minimizes the population L^2 error

$$\operatorname{argmin}_{\beta \in \mathbb{R}^N} \|f_i^{(k)} - \beta^\top \psi\|_{\mathcal{H}}^2.$$

By observing that the optimal coefficients to minimize the L^2 error are the PCE coefficients in Lemma 1, we have

$$\|f_i^{(k)} - E_{k,i}^* \top \psi\|_{\mathcal{H}} \leq C_{s,n_x} p^{-s} \|f_i^{(k)}\|_{H_\mu^s(\Omega)}.$$

Let $E_{k,i}$ denote the i th row of E_k . Then $E_{k,i}$ minimizes the empirical L^2 loss problem (55). By Lemma 2, since $|f_i^{(k)}| \leq 1$ as $\Omega = [-1, 1]^{n_x}$, we obtain w.h.p.,

$$\|f_i^{(k)} - E_{k,i}^* \top \psi\|_{\mathcal{H}}^2 - \|f_i^{(k)} - E_{k,i}^\top \psi\|_{\mathcal{H}}^2 \leq C_l \frac{N^2 \log M_m}{M_m}, \quad (57)$$

which implies that

$$\begin{aligned} \|f_i^{(k)} - E_{k,i}^* \top \psi\|_{\mathcal{H}} &\leq \sqrt{C_{s,n_x}^2 p^{-2s} \|f_i^{(k)}\|_{H_\mu^s(\Omega)}^2 + C_l \frac{N^2 \log M_m}{M_m}} \\ &\leq C_{s,n_x} p^{-s} \|f_i^{(k)}\|_{H_\mu^s(\Omega)} + \sqrt{C_l \frac{N^2 \log M_m}{M_m}} \end{aligned}$$

which completes the proof.

4.3 Comparison of single-step and multi-step EDMD

The error bounds (43) and (56) show that learning the condensed formulation in multi-step EDMD fundamentally alters the way that the learning error propagates through the prediction horizon. Specifically, in conventional single-step EDMD, (43) shows that the learning error accumulates due to the repeated composition of the approximate Koopman operator $\mathcal{K}_{N,M}$. This is reflected by the factor $\|\mathcal{K}_{N,M}\|_{\mathcal{H}}^\ell$ that amplifies the single-step error $\text{Err}_{N,M}^{\text{ss}}(f_i^{(k-1-\ell)})$ in (43). In the event that $\|\mathcal{K}_{N,M}\|_{\mathcal{H}} > 1$ or the spectral radius $\rho(A_{N,M}) > 1$, even low single-step errors can lead to significant degradation in long-horizon predictions as a result of this amplification. This phenomenon is also observed in our case studies in Section 6 involving two different nonlinear oscillators.

On the other hand, the condensed multi-step EDMD operator directly approximates the input-output mapping $f^{(k)}$, thereby avoiding the artificial accumulation of error due to repeated composition of the learned operator. As a result, the error bound in (56) depends only on the approximation quality of the multi-step map $f^{(k)}$ and the number of data trajectories M_m , which does not degrade with the length of the prediction horizon. This fundamental structural difference in the learning method explains the improved performance of multi-step EDMD in practice and motivates the usage of multi-step EDMD in long-horizon prediction and MPC.

It is important to note that in the multi-step EDMD formulation, each data trajectory effectively contributes one training sample for learning the condensed matrices. This reflects a fundamental tradeoff between expressivity and variance, since multi-step EDMD reduces error accumulation across the prediction horizon at the cost of increased data requirements. In applications where a dynamic model of the nonlinear system is available, this is typically not restrictive, as data can be generated at a low cost.

5 Practical Guidelines

The preceding sections and theoretical analyses provide insights into practical guidelines for multi-step EDMD applications in MPC.

5.0.0.1 Offline learning, Online MPC We reiterate that the multi-step EDMD operator is learned offline before integration with MPC. During MPC, the observables $z_0 = \psi(x_0)$ is only computed once per Condensed Koopman-MPC problem (10). This substantially reduces the online computational burden of having a high-dimensional Koopman lifting N .

5.0.0.2 Pre-computation in Parallelized Sub-problems The multi-step EDMD learning process can be further accelerated by parallelizing the multi-step prediction error minimization problem (15). Specifically, we can write (15) as

$$\min_{E_{k,i}, F_{k,i}} f_{k,i}(E_{k,i}, F_{k,i}) = \|\mathbf{G}E_{k,i} + \mathbf{H}_k F_{k,i} - h_k^i\|_2^2 \quad (58)$$

where

$$\mathbf{G} := \begin{bmatrix} \psi(x_{1,0})^\top \\ \vdots \\ \psi(x_{M_m,0})^\top \end{bmatrix}, \quad \mathbf{H}_k := \begin{bmatrix} u_{1,0}^\top & \cdots & u_{1,k-1}^\top \\ \vdots & & \vdots \\ u_{M_m,0}^\top & \cdots & u_{M_m,k-1}^\top \end{bmatrix}, \quad (59)$$

and

$$h_k^i := \begin{bmatrix} x_{1,k}^i & \cdots & x_{M_m,k}^i \end{bmatrix}^\top. \quad (60)$$

Importantly, \mathbf{G} can be pre-computed only once and reused for every horizon, and \mathbf{H}_k can be pre-computed once per horizon for every state coordinate. This can accelerate the learning process when the number of trajectories M_m is very large.

5.0.0.3 Elastic net regularization and pruning

Our theoretical analysis assumed that the observables $\{\psi_i\}_{i=1}^N$ are orthonormal with respect to the sampled distribution μ . In practice, this assumption could be violated in higher-dimensional settings such as discretizations of PDE systems, where spatially neighboring states are strongly correlated. As a result, the empirical L^2 error regression problems may be highly ill-conditioned, which may lead to numerical instability during the learning process. To mitigate this issue, we can employ elastic-net regularization when learning the multi-step EDMD operators. Formally, the regularized problem is

$$\begin{aligned} \min_{E_{k,i}, F_{k,i}} \quad & f_{k,i}(E_{k,i}, F_{k,i}) = \\ & \|\mathbf{G}E_{k,i} + \mathbf{H}_k F_{k,i} - h_k^i\|_2^2 + \beta \left\| \begin{bmatrix} E_{k,i} \\ F_{k,i} \end{bmatrix} \right\|_2^2 + \tau \|E_{k,i}\|_1 \end{aligned} \quad (61)$$

where $\beta > 0$ and $\tau > 0$ are ℓ_2 and ℓ_1 regularization parameters respectively. The ℓ_2 regularization improves numerical conditioning, while the ℓ_1 regularization promotes sparsity of the resulting multi-step EDMD model [34,47]. Additionally, an optional pruning step can be performed to remove observables with negligible contribution to the learned dynamics. This step improves interpretability and reduces computation time for the multi-step EDMD operator while preserving prediction accuracy. An example of a straightforward multi-step EDMD learning algorithm with elastic net regularization and pruning is provided in Algorithm 1 in Appendix C.

Importantly, these regularization and pruning steps are optional and do not structurally change the multi-step EDMD learning method for MPC. They serve as add-ons to improve the numerical stability and scaling performance of the multi-step EDMD framework.

5.0.0.4 Model complexity and data availability

The error bound in (56) explicitly depends on the observable dimensionality N and the number of data trajectories M_m . While increasing N decreases the projection error (bias), it increases the regression error (variance), which is a concrete example of a bias-variance trade-off. Consequently, the multi-step EDMD model performance requires balancing model expressivity with data

availability, ideally with $M_m \gg N^2$. Importantly, when a dynamic model of the nonlinear system is available, multi-step EDMD is particularly effective since data trajectories can be generated readily, and data scarcity is not a limiting factor.

6 Numerical Experiments

This section evaluates our proposed multi-step Koopman MPC framework in two benchmark numerical case studies of two highly nonlinear oscillators: Van der Pol and Duffing. These two illustrative examples provide insight into the performance of our framework across different dynamical regimes. For each nonlinear oscillator, we compare the performance of three different predictors:

- (1) One-step EDMD
- (2) Multi-step Koopman Predictor
- (3) Multi-step Koopman Predictor with pruning

These two case studies demonstrate the efficacy of our multi-step Koopman framework in two distinct dynamical regimes. All numerical results can be reproduced with the code found in the <https://github.com/SOLARIS-JHU/Multi-step-Koopman>.

6.1 Van der Pol oscillator

Consider the Van Der Pol Oscillator with forced dynamics,

$$\begin{aligned} \dot{x}_1 &= x_2, \\ \dot{x}_2 &= \mu(1 - x_1^2)x_2 - \omega_0^2 x_1 + u, \end{aligned} \quad (62)$$

where $x := [x_1, x_2]^\top$ is the state vector, $\mu = 5$ is a damping parameter, and $\omega_0 = 0.8$ is the natural frequency of the oscillator. For these simulations, a relatively large value for μ was chosen so that the oscillator exhibits strong nonlinear behavior with different time scales in the charging and discharging phases.

6.1.1 Open-loop performance

To obtain the dataset for training each predictor, $M_m = 2 \times 10^5$ short trajectories of the oscillator were simulated, each with $H = 20$ time steps of length $T_S = 0.01$, where H denotes the length of the prediction horizon. The initial states x_0 were uniformly sampled in the box $[-2, 2]^2 \subset \mathbb{R}^2$. The oscillator was simulated using the fourth-order Runge-Kutta method. The control trajectories were sampled using a pseudo-random binary sequence with values in $\pm U_{\text{amp}} = \pm 0.5$, to ensure sufficient excitation of the oscillator. We used an observable map ψ consisting of the (scaled) Legendre polynomials of total degree $d \leq 10$, which results in a lifted space dimension of $N = 66$. The threshold weight for pruning the multi-step model was set to $\epsilon_E = 10^{-3}$. The metric used

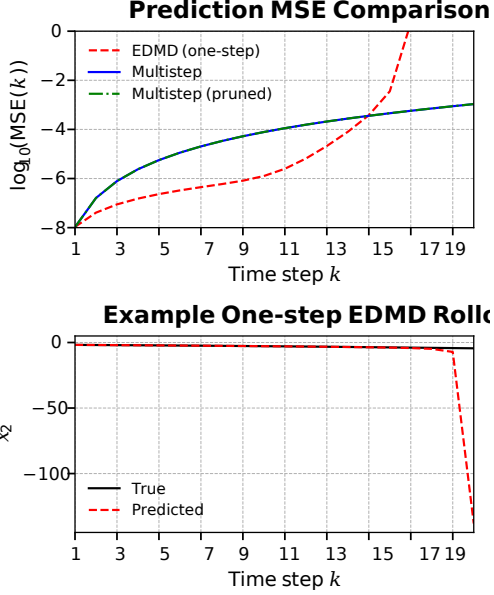


Fig. 1. Top: Prediction MSE comparison across different models for the van der Pol oscillator. Bottom: Example x_2 trajectory prediction which one-step EDMD, which diverges over longer horizons.

to compare the different predictors is the mean-squared error (MSE), which is defined for various timesteps k as

$$\text{MSE}(k) = \frac{1}{M_m} \sum_{j=1}^{M_m} \|x_{\text{true}}(kT_s) - x_{\text{pred}}(kT_s)\|^2. \quad (63)$$

Fig. 1 shows the mean-squared error at each timestep k for various predictors. Our multi-step Koopman predictors are far more accurate than conventional EDMD, especially in the later parts of the prediction horizon, where the MSE for conventional EDMD diverges to infinity. This phenomenon in conventional EDMD is attributed to the exponential growth of the spectral radius of $A_{N,M}^k$ ($\rho(A_{N,M}) = 1.38$), whereas the multi-step Koopman model mitigates this effect by capturing the nonlinear dynamics over longer time intervals. Some sample trajectories illustrating this phenomenon are also shown in Fig. 1. The variant with pruning yields nearly identical MSE while reducing the dimensionality of the lift to $N = 25$, which shows that redundant observables can be removed without significant loss of performance.

6.1.2 Closed-loop performance

The conventional one-step Koopman model exhibited numerical instability during open-loop prediction, which renders it completely unsuitable for integration with MPC for closed-loop evaluation. This highlights a fundamental limitation of one-step Koopman models under dynamic regimes with strong nonlinearities.

In contrast, the multi-step Koopman models remained numerically stable during prediction, and we integrated the models with MPC to regulate the oscillator to the origin. At each time step, we solve the Condensed Koopman-MPC problem (10). Specifically, at each time step, we solve the MPC problem (10) with the settings $u_{\min} = -10$, $u_{\max} = 10$, $Q = I_N$, and $R = 0.01I_m$, and no state constraints. Fig. 2 shows the state trajectories for both multi-step models and the control trajectories. The resulting controller was able to stabilize the oscillator gradually while ensuring that input constraints were satisfied.

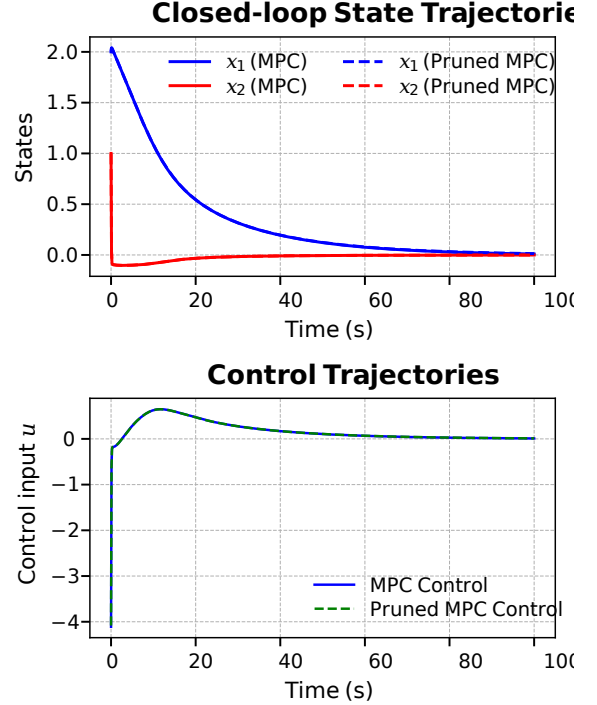


Fig. 2. Closed-loop state (top) and control (bottom) trajectories for the van der Pol oscillator.

6.2 Duffing Oscillator

We consider another canonical case study involving the Duffing oscillator. The dynamics of the Duffing oscillator are given by

$$\begin{aligned} \dot{x}_1 &= x_2, \\ \dot{x}_2 &= -\delta x_2 - \alpha x_1 - \beta x_1^3 + u, \end{aligned} \quad (64)$$

where $x := [x_1, x_2]^\top \in \mathbb{R}^2$ is the state vector, $u \in \mathbb{R}$ is the control action, and the parameters $\delta = 0.2$, $\alpha = -1$, $\beta = 1$. For this set of parameters, the Duffing oscillator exhibits highly nonlinear restoring forces with multiple equilibrium basins. Notably, it can be shown that for the autonomous case $u = 0$, $x = [0, 0]^\top$ is an unstable equilibrium point, whereas $x = [\pm 1, 0]^\top$ are stable equilibrium points. The unstable equilibrium point admits a separatrix (stable manifold) that divides the state space

into two basins of attractions for the two stable equilibria. Consequently, long-horizon predictions starting the near the separatrix are particularly challenging. See Fig. 5 for an illustration.

6.2.1 Open-loop performance

Similar to the previous case study, to obtain the dataset for training each predictor, $M_m = 2 \times 10^3$ long trajectories of the oscillator were simulated, each with $H = 50$ time steps of length $T_S = 0.025$, where H denotes the length of the prediction horizon. We used an observable map ψ consisting of the (scaled) Legendre polynomials of total degree $d \leq 14$, which results in a lifted space dimension of $N = 120$. The oscillator was simulated using the fourth-order Runge-Kutta method. The control trajectories were sampled using a pseudo-random binary sequence with values in $\pm U_{\text{amp}} = \pm 1$ to ensure sufficient excitation. For the pruned multi-step model, the threshold weight was set to $\epsilon_E = 10^{-2}$. The sampling method for x_0 , and the metric for model comparison for various timesteps are the same as the ones in the previous case study.

Fig. 3 shows the mean-squared error at each timestep k for various predictors. We observe the same phenomenon whereby the single-step EDMD predictors diverge after $k = 20$ timesteps, whereas the predictions made by multi-step EDMD remain stable for longer horizons. This phenomenon is again attributed to the exponential growth of the spectral radius of $A_{N,M}^k$ ($\rho(A_{N,M}) = 2.5$) for single-step EDMD, which amplifies prediction errors made in earlier timesteps. Furthermore, the variant with pruning yields nearly identical MSE while reducing the dimensionality of the lift from $N = 120$ to $N = 13$, which shows that redundant observables can be removed without significant loss of performance.

6.2.2 Closed-loop performance

Similar to the previous case study, the conventional one-step Koopman model exhibited numerical instability during open-loop prediction for longer horizons; that is, single-step EDMD-MPC fails if choosing longer horizons. To enable a fair and well-posed comparison with our multi-step models in MPC integration, we truncated the prediction horizon for single-step EDMD to $H = 10$.

At each time step, we solve the Condensed Koopman-MPC problem (10), with the settings $u_{\min} = -1$, $u_{\max} = 1$, $Q = I_N$, and $R = 0.01I_m$, and no state constraints. Fig. 4 shows the state trajectories for all models and the control trajectories. The resulting controllers from the multi-step models were able to stabilize the oscillator gradually while ensuring that input constraints were satisfied. In contrast, the single-step EDMD-based controllers exhibit frequent excitations and transitions between the two stable equilibrium points. This behavior

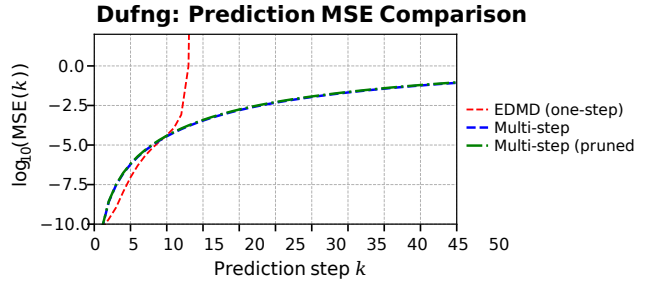


Fig. 3. Prediction MSE comparison for the Duffing oscillator across different models.

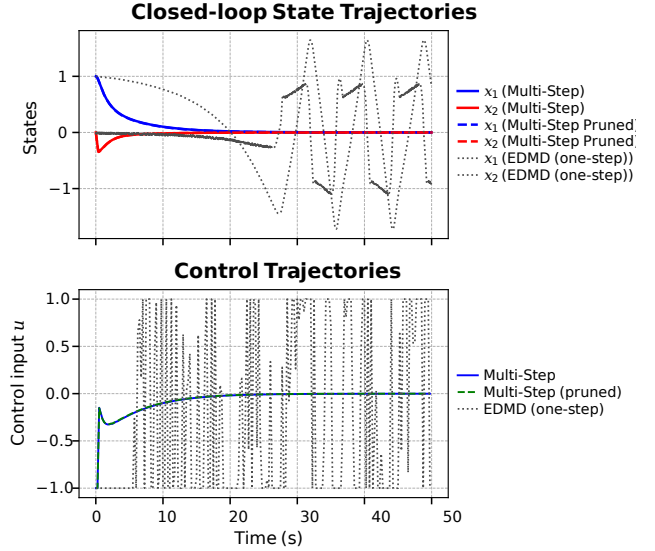


Fig. 4. Closed-loop state (top) and control (bottom) trajectories for the oscillator.

is consistent with the poor long-horizon predictions of the one-step predictor, particularly near the separatrix of the dynamics, where small perturbations lead to large deviations in the long-horizon behavior. The phase portraits for all closed-loop simulations are shown in Fig. 5.

Overall, the open- and closed-loop simulations demonstrate that the multi-step Koopman operators are far superior in terms of predictive accuracy and stable MPC operation than one-step predictors in strongly nonlinear dynamical regimes. The pruning process also enables the removal of redundant observables in the multi-step predictor and does not significantly affect the predictive accuracy or closed-loop performance of our multi-step Koopman predictors.

7 Conclusion

This paper proposes a multi-step EDMD framework for Koopman-based MPC that directly learns the condensed multi-step state-control mapping required for QP-based MPC formulations. The proposed approach preserves a convex least-squares structure while aligning the learning objective with the finite-horizon nature of MPC.

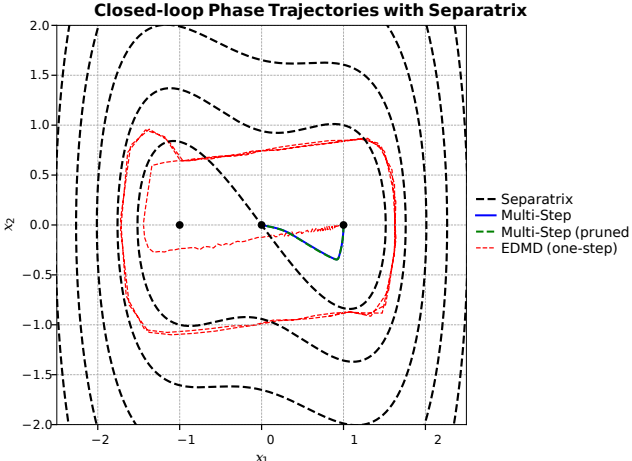


Fig. 5. Closed-loop phase trajectories of the Duffing oscillator with separatrix. The separatrix separates the two basins of attraction of the equilibria (black dots). Multi-step MPC and its pruned variant converge to the origin, while single-step MPC crosses the separatrix, leading to poor closed-loop behavior.

We further showed that the identification problem decomposes across prediction horizons and state coordinates, enabling parallelized computation and row-wise ℓ_1 -regularization for automatic dictionary pruning. A non-asymptotic error analysis provides a rigorous explanation for the observed improved performance of the proposed multi-step EDMD for long-horizon predictions. Numerical simulations on the van der Pol oscillator and the Duffing oscillator demonstrate that our framework achieves low multi-step prediction errors and effective closed-loop state regulation compared to conventional EDMD. Future work aims to analyze stochastic extensions of the multi-step Koopman operator [44,5] and integrate the framework with Stochastic MPC (SMPC) formulations [22,12].

References

- [1] Mohammad Abtahi, Mahdis Rabbani, Armin Abdolmohammadi, and Shima Nazari. Multi-step deep Koopman network (MDK-net) for vehicle control in Frenet frame. *arXiv preprint arXiv:2503.03002*, 2025.
- [2] Hassan Arbabi, Milan Korda, and Igor Mezić. A data-driven Koopman model predictive control framework for nonlinear partial differential equations. In *Proceedings of the IEEE Conference on Decision and Control*, pages 6409–6414, 2018.
- [3] Julian Berberich, Johannes Köhler, Matthias A Müller, and Frank Allgöwer. Linear tracking MPC for nonlinear systems—Part i: The model-based case. *IEEE transactions on automatic control*, 67(9):4390–4405, 2022.
- [4] Claudio Canuto and Alfio Quarteroni. Approximation results for orthogonal polynomials in Sobolev spaces. *Mathematics of Computation*, 38(157):67–86, 1982.
- [5] Nelida Črnjarić-Žic, Senka Maćesić, and Igor Mezić. Koopman operator spectrum for random dynamical systems. *Journal of Nonlinear Science*, 30(5):2007–2056, 2020.
- [6] Steven Dahdah and James R Forbes. System norm regularization methods for Koopman operator approximation. *Proceedings of the Royal Society A*, 478(2265):20220162, 2022.
- [7] Thomas de Jong, Valentina Breschi, Maarten Schoukens, and Mircea Lazar. Koopman data-driven predictive control with robust stability and recursive feasibility guarantees. In *IEEE 63rd Conference on Decision and Control*, pages 140–145, 2024.
- [8] Loris Di Natale, Muhammad Zakwan, Bratislav Svetozarevic, Philipp Heer, Giancarlo Ferrari-Trecate, and Colin N Jones. Stable linear subspace identification: A machine learning approach. In *Proceedings of the 2024 European Control Conference (ECC)*, pages 3539–3544. IEEE, 2024.
- [9] Hans Joachim Ferreau, Christian Kirches, Andreas Potschka, Hans Georg Bock, and Moritz Diehl. qpOASES: A parametric active-set algorithm for quadratic programming. *Mathematical Programming Computation*, 6(4):327–363, 2014.
- [10] S. Gros, M. Zanon, R. Quirynen, A. Bemporad, and M. Diehl. From linear to nonlinear MPC: Bridging the gap via the real-time iteration. *International Journal of Control*, 93(1):62–80, 2020.
- [11] Yue Guo, Milan Korda, Ioannis G Kevrekidis, and Qianxiao Li. Learning parametric Koopman decompositions for prediction and control. *SIAM Journal on Applied Dynamical Systems*, 24(1):744–781, 2025.
- [12] Tor Aksel N Heirung, Joel A Paulson, Jared O’Leary, and Ali Mesbah. Stochastic model predictive control—how does it work? *Computers & Chemical Engineering*, 114:158–170, 2018.
- [13] Maximiliano Hertel, Friedrich M. Philipp, Manuel Schaller, and Karl Worthmann. Koopman for stochastic dynamics: error bounds for kernel extended dynamic mode decomposition. *arXiv preprint arXiv:2512.20247*, 2025.
- [14] B.O. Koopman. Hamiltonian systems and transformation in Hilbert space. *Proceedings of the National Academy of Sciences*, 17(5):315–318, 1931.
- [15] M. Korda and I. Mezić. Linear predictors for nonlinear dynamical systems: Koopman operator meets model predictive control. *Automatica*, 93:149–160, 2018.
- [16] Milan Korda and Igor Mezić. On convergence of extended dynamic mode decomposition to the Koopman operator. *Journal of Nonlinear Science*, 28(2):687–710, 2018.
- [17] Milan Korda and Igor Mezić. Optimal construction of Koopman eigenfunctions for prediction and control. *IEEE Transactions on Automatic Control*, 65(12):5114–5129, 2020.
- [18] Mircea Lazar. Basis-functions nonlinear data-enabled predictive control: Consistent and computationally efficient formulations. In *Proceedings of the European Control Conference*, pages 888–893, 2024.
- [19] Qianxiao Li, Felix Dietrich, Erik M Boltt, and Ioannis G Kevrekidis. Extended dynamic mode decomposition with dictionary learning: A data-driven adaptive spectral decomposition of the Koopman operator. *Chaos: An Interdisciplinary Journal of Nonlinear Science*, 27(10), 2017.
- [20] Alexandre Mauroy and Jorge Goncalves. Koopman-based lifting techniques for nonlinear systems identification. *IEEE Transactions on Automatic Control*, 65(6):2550–2565, 2019.
- [21] Alexandre Mauroy and Igor Mezić. Global stability analysis using the eigenfunctions of the Koopman operator. *IEEE Transactions on Automatic Control*, 61(11):3356–3369, 2016.

[22] Ali Mesbah. Stochastic model predictive control: An overview and perspectives for future research. *IEEE Control Systems Magazine*, 36(6):30–44, 2016.

[23] Feliks Nüske, Sebastian Peitz, Friedrich Philipp, Manuel Schaller, and Karl Worthmann. Finite-data error bounds for Koopman-based prediction and control. *Journal of Nonlinear Science*, 33(14):1–34, 2023.

[24] Friedrich M. Philipp, Manuel Schaller, Septimus Boshoff, Sebastian Peitz, Feliks Nüske, and Karl Worthmann. Variance representations and convergence rates for data-driven approximations of Koopman operators. *arXiv preprint arXiv:2402.02494*, 2024.

[25] Friedrich M. Philipp, Manuel Schaller, Karl Worthmann, Sebastian Peitz, and Feliks Nüske. Error bounds for kernel-based approximations of the koopman operator. *Applied and Computational Harmonic Analysis*, 71:101657, 2024.

[26] J.L. Proctor, S.L. Brunton, and J.N. Kutz. Generalizing Koopman theory to allow for inputs and control. *SIAM Journal on Applied Dynamical Systems*, 17(1):909–930, 2018.

[27] James Blake Rawlings, David Q Mayne, Moritz Diehl, et al. *Model predictive control: theory, computation, and design*, volume 2. Nob Hill Publishing Madison, WI, 2020.

[28] Omar Sayed and Sergio Lucia. A novel Koopman representation for efficient linear model predictive control of nonlinear systems. In *2024 European Control Conference (ECC)*, pages 3570–3575. IEEE, 2024.

[29] Omar Sayed and Sergio Lucia. Recursive least squares-based identification for multi-step Koopman operators. In *Proceedings of the European Control Conference*, pages 941–946, 2024.

[30] Haojie Shi and Max Q-H Meng. Deep Koopman operator with control for nonlinear systems. *IEEE Robotics and Automation Letters*, 7(3):7700–7707, 2022.

[31] Bartolomeo Stellato, Goran Banjac, Paul Goulart, Alberto Bemporad, and Stephen Boyd. OSQP: An operator splitting solver for quadratic programs. *Mathematical Programming Computation*, 12(4):637–672, 2020.

[32] Robin Strässer, Karl Worthmann, Igor Mezić, Julian Berberich, Manuel Schaller, and Frank Allgöwer. An overview of Koopman-based control: From error bounds to closed-loop guarantees. *Annual Reviews in Control*, 61:101035, 2026.

[33] H-T Su and TJ McAvoy. Neural model predictive control of nonlinear chemical processes. In *Proceedings of 8th IEEE International Symposium on Intelligent Control*, pages 358–363. IEEE, 1993.

[34] W. Sun and R. D. Braatz. Alven: Algebraic learning via elastic net for static and dynamic nonlinear model identification. *Computers and Chemical Engineering*, 143, 2020.

[35] Gábor Szegő. *Orthogonal Polynomials*, volume 23. American Mathematical Soc., New York, 1939.

[36] Roman Vershynin. *High-Dimensional Probability: An Introduction with Applications in Data Science*. Cambridge University Press, UK, 2018.

[37] M.O. Williams, M.S. Hemati, S.T.M. Dawson, I.G. Kevrekidis, and C.W. Rowley. Extending data-driven Koopman analysis to actuated systems. *IFAC-PapersOnLine*, 49(18):704–709, 2016.

[38] M.O. Williams, I.G. Kevrekidis, and C.M. Rowley. A data-driven approximation of the Koopman operator: Extending dynamic mode decomposition. *Journal of Nonlinear Science*, 25:1307–1346, 2015.

[39] L. Wu, Y. Che, R. D. Braatz, and J. Drgona. A Time-certified Predictor-corrector IPM Algorithm for Box-QP. *IEEE Control System Letters*, pages 1–16, 2025. DOI: 10.1109/LCSYS.2025.3647842.

[40] L. Wu, W. Xiao, and R. D. Braatz. EIQP: Execution-time-certified and Infeasibility-detecting QP solver. *IEEE Transactions on Automatic Control*, pages 1–16, 2025. DOI: 10.1109/TAC.2025.3631575.

[41] Liang Wu and Alberto Bemporad. A Simple and Fast Coordinate-Descent Augmented-Lagrangian Solver for Model Predictive control. *IEEE Transactions on Automatic Control*, 68(11):6860–6866, 2023.

[42] Liang Wu and Richard D. Braatz. A Direct Optimization Algorithm for Input-Constrained MPC. *IEEE Transactions on Automatic Control*, 70(2):1366–1373, 2025.

[43] Yongqian Xiao, Xinglong Zhang, Xin Xu, Xueqing Liu, and Jiahang Liu. Deep neural networks with Koopman operators for modeling and control of autonomous vehicles. *IEEE transactions on intelligent vehicles*, 8(1):135–146, 2022.

[44] Yuanchao Xu, Kaidi Shao, Isao Ishikawa, Yuka Hashimoto, Nikos Logothetis, and Zhongwei Shen. A data-driven framework for Koopman semigroup estimation in stochastic dynamical systems. *arXiv preprint arXiv:2501.13301*, 2025.

[45] Enoch Yeung, Soumya Kundu, and Nathan Hudas. Learning deep neural network representations for Koopman operators of nonlinear dynamical systems. In *Proceedings of the American Control Conference*, pages 4832–4839, 2019.

[46] Christophe Zhang and Enrique Zuazua. A quantitative analysis of Koopman operator methods for system identification and predictions. *Comptes Rendus. Mécanique*, 351:1–31, 12 2022.

[47] Hui Zou and Trevor Hastie. Regularization and variable selection via the elastic net. *Journal of the Royal Statistical Society Series B: Statistical Methodology*, 67(2):301–320, 2005.

A Proof of Lemma 2

First, we prove that the Legendre polynomials satisfy a Euclidean norm growth bound.

Lemma 3 $\|\psi(x)\|_2 \leq (p+1)^{n_x} = N \mu\text{-almost surely.}$

Proof 5 Let $\phi_\alpha(x)$ be the k th Legendre polynomial defined in (29). Note that

$$\sup_{x \in [-1,1]} \phi_\alpha(x) = \phi_\alpha(1) = \sqrt{2k+1}$$

which follows from Eq. 7.21.1 in [35]. Let $\psi(x) = [\phi_0(x), \phi_1(x), \dots, \phi_p(x)]$. For $n_x = 1$, the statement now follows from a direct computation:

$$\sup_{x \in [-1,1]} \|\psi(x)\|_2^2 = \|\psi(1)\|_2^2 = \sum_{\alpha=0}^p (2k+1) = (p+1)^2. \quad (\text{A.1})$$

For arbitrary n_x , note that

$$\psi(x) = \psi(x^1) \otimes \psi(x^2) \otimes \dots \otimes \psi(x^{n_x}), \quad (\text{A.2})$$

and hence

$$\begin{aligned} \sup_{x \in [-1,1]^{n_x}} \|\psi(x)\|_2^2 &= \|\psi(1) \otimes \psi(1) \otimes \cdots \otimes \psi(1)\|_2^2 \\ &= (p+1)^{2n_x}. \end{aligned}$$

Proof of Lemma 2: Let $N = (p+1)^{n_x}$ and define $\psi_j := \psi(x_j)$. By orthonormality of the PCE basis, $\mathbb{E}[\psi_j \psi_j^\top] = I_N$. Moreover, Lemma 3 implies $\|\psi_j\|_2 \leq N$ almost surely. Define $Z_j := \psi_j \psi_j^\top - I_N$. Then $\mathbb{E}[Z_j] = 0$ and $\|Z_j\| \leq \|\psi_j\|_2^2 + 1 \leq N^2 + 1$. Furthermore,

$$\mathbb{E}[Z_j^2] = \mathbb{E}[\|\psi_j\|_2^2 \psi_j \psi_j^\top] - I_N.$$

For any unit vector $u \in \mathbb{R}^N$,

$$u^\top \mathbb{E}[Z_j^2] u \leq N^2 \mathbb{E}[(u^\top \psi_j)^2] - 1 = N^2 - 1,$$

and hence $\|\mathbb{E}[Z_j^2]\| \leq N^2 - 1$. Therefore,

$$\left\| \sum_{i=1}^M \mathbb{E}[Z_j^2] \right\| \leq M(N^2 - 1).$$

By the Matrix Bernstein Inequality (Thm. 5.4.1 in [36]), there exists a universal constant \tilde{C} such that, with probability at least $1 - \delta$,

$$\|\widehat{\Sigma} - I_N\| \leq \tilde{C} \left(\frac{N^2}{M} \log \frac{2N}{\delta} + \sqrt{\frac{N^2}{M} \log \frac{2N}{\delta}} \right) =: \eta.$$

For $\eta < 1$, this inequality implies that

$$\|\widehat{\Sigma}^{-1} - I_N\| \leq \frac{\eta}{1 - \eta}.$$

Next, define $g := \mathbb{E}[\psi_j y_j]$. For any unit vector $u \in \mathbb{R}^N$,

$$|u^\top g| \leq \sqrt{\mathbb{E}[y_j^2] \mathbb{E}[(u^\top \psi_j)^2]} \leq M_y,$$

so $\|g\|_2 \leq M_y$. Define $v_j := \psi_j y_j - g$. Let

$$V_j := \begin{bmatrix} 0 & v_j^\top \\ v_j & 0 \end{bmatrix}.$$

Then $\mathbb{E}[V_j] = 0$ and $\|V_j\| \leq \|V_j\|_F \leq 2M_y N$. Moreover, $\|V_j^2\| \leq 4M_y^2 N^2$, yielding

$$\left\| \sum_{i=1}^M \mathbb{E}[V_j^2] \right\| \leq 4M_y^2 MN^2.$$

Applying the Matrix Bernstein inequality again gives, with probability $1 - \delta$,

$$\|\widehat{g} - g\|_2 \leq 2\tilde{C} \left(\frac{M_y N}{M} \log \frac{2N}{\delta} + \sqrt{\frac{M_y^2 N^2}{M} \log \frac{2N}{\delta}} \right).$$

Set $\delta = M^{-2}$. Then, with probability $1 - 2M^{-2}$,

$$\begin{aligned} \|\widehat{\beta} - \beta_\star\|_2 &\leq \|\widehat{\Sigma}^{-1} - I_N\| \|g\|_2 + \|\widehat{\Sigma}^{-1}\| \|\widehat{g} - g\|_2 \\ &\leq \frac{\eta}{1 - \eta} M_y + \left(1 + \frac{\eta}{1 - \eta} \right) \|\widehat{g} - g\|_2 \\ &= C_l \left(\sqrt{\frac{M_y^2 N^2 \log M}{M}} \right), \quad M \gg N^2, \end{aligned}$$

for some universal constant \tilde{C}_l . Finally, since $\Sigma = I_N$,

$$\begin{aligned} &\|y - \widehat{\beta}^\top \psi\|_{\mathcal{H}}^2 - \|y - \beta_\star^\top \psi\|_{\mathcal{H}}^2 \\ &= \mathbb{E}[(y - \widehat{\beta}^\top \psi(x))^2] - \mathbb{E}[(y - \beta_\star^\top \psi(x))^2] \\ &\leq (\widehat{\beta} - \beta_\star)^\top \Sigma (\widehat{\beta} - \beta_\star) \\ &= \|\widehat{\beta} - \beta_\star\|_2^2 = C_l \left(\frac{M_y^2 N^2 \log M}{M} \right) \end{aligned}$$

for some universal constant C_l .

B Proof of Theorem 1

We first decompose the error as

$$\begin{aligned} \|\mathcal{K}g - \mathcal{K}_{N,M}g\|_{\mathcal{H}} &\leq \|\mathcal{K}(g - P_N g)\|_{\mathcal{H}} + \|\mathcal{K}P_N g - \mathcal{K}_{N,M}g\|_{\mathcal{H}} \\ &= \|\mathcal{K}(g - P_N g)\|_{\mathcal{H}} + \|(\mathcal{K} - \mathcal{K}_{N,M})P_N g\|_{\mathcal{H}} \end{aligned}$$

The second equality follows because $\mathcal{K}_{N,M}g = P_{N,M}\mathcal{K}P_N g = P_{N,M}\mathcal{K}P_N^2 g = \mathcal{K}_{N,M}P_N g$. The first term is known as the approximation error, and can be bounded using Lemma 1 with $q = 0$:

$$\begin{aligned} \|\mathcal{K}(g - P_N g)\|_{\mathcal{H}} &\leq \|\mathcal{K}\|_{\mathcal{H}} \|(g - P_N g)\|_{\mathcal{H}} \\ &\leq C_{s,n_x} p^{-s} \|\mathcal{K}\|_{\mathcal{H}} \|g\|_{H_\mu^s(\Omega)}. \end{aligned} \quad (\text{B.1})$$

The second term can be further bounded as

$$\|(\mathcal{K} - \mathcal{K}_{N,M})P_N g\|_{\mathcal{H}} \leq \|(\mathcal{K} - \mathcal{K}_N)P_N g\|_{\mathcal{H}} + \|(\mathcal{K}_N - \mathcal{K}_{N,M})P_N g\|_{\mathcal{H}}. \quad (\text{B.2})$$

The first and second terms on the right-hand side are known as the bias and variance error, respectively. The bias term can again be bounded using Lemma 1 with

$q > 0$:

$$\begin{aligned}\|(\mathcal{K} - \mathcal{K}_N)P_N g\|_{\mathcal{H}} &= \|(I - P_N)\mathcal{K}P_N g\|_{\mathcal{H}} \\ &= \|(I - P_N)((P_N g) \circ f)\|_{\mathcal{H}} \\ &\leq C_{s,n_x} p^{-q} \|(P_N g) \circ f\|_{H_{\mu}^q(\Omega)} \\ &= C_{s,n_x} p^{-q} \|\mathcal{K}\|_{H_{\mu}^q(\Omega)} \|P_N g\|_{H_{\mu}^q(\Omega)}\end{aligned}$$

By noting that

$$\begin{aligned}\|P_N g\|_{H_{\mu}^q(\Omega)} &\leq \|g\|_{H_{\mu}^q(\Omega)} + \|(I - P_N)g\|_{H_{\mu}^q(\Omega)} \\ &= \|g\|_{H_{\mu}^q(\Omega)} + C_{s,n_x} p^{2q-s-\frac{1}{2}} \|g\|_{H_{\mu}^s(\Omega)},\end{aligned}$$

we have that

$$\begin{aligned}\|(\mathcal{K} - \mathcal{K}_N)P_N g\|_{\mathcal{H}} &\leq C_{s,n_x} p^{-q} \|\mathcal{K}\|_{H_{\mu}^q(\Omega)} \left(\|g\|_{H_{\mu}^q(\Omega)} \right. \\ &\quad \left. + C_{s,n_x} p^{2q-s-\frac{1}{2}} \|g\|_{H_{\mu}^s(\Omega)} \right).\end{aligned}\quad (\text{B.3})$$

It now remains to bound the variance error $\|(\mathcal{K}_N - \mathcal{K}_{N,M})P_N g\|_{\mathcal{H}}$. Write $P_N g = \sum_{l=1}^N c_l \psi_l$. Then we have, by the Cauchy-Schwarz Inequality,

$$\|(\mathcal{K}_N - \mathcal{K}_{N,M})P_N g\|_{\mathcal{H}}^2 \leq N \sum_{l=1}^N c_l^2 \|(\mathcal{K}_N - \mathcal{K}_{N,M})\psi_l\|_{\mathcal{H}}^2. \quad (\text{B.4})$$

We now apply Lemma 2 for each basis function ψ_l by defining the response $y = \mathcal{K}_N \psi_l = P_N(\psi_l \circ f)$. Note that we have $|y| \leq B_{f,N}$ μ -almost surely, and also,

$$\mathcal{K}_{N,M} \psi_l = \beta^{(l)\top} \psi \quad (\text{B.5})$$

where $\beta^{(l)}$ is the k th row of the EDMD matrix $A_{N,M}$ that minimizes the empirical L^2 loss. Furthermore, if $\beta_*^{(l)}$ minimizes the population loss, then

$$\|y - \beta_*^{(l)} \psi\|_{\mathcal{H}}^2 = 0 \quad (\text{B.6})$$

because $y = P_N(\psi_l \circ f) \in \mathcal{F}_N$. By Lemma 2, we obtain w.h.p.,

$$\begin{aligned}\|(\mathcal{K}_N - \mathcal{K}_{N,M})\psi_l\|_{\mathcal{H}}^2 &= \|y - \beta_*^{(l)} \psi\|_{\mathcal{H}}^2 \\ &\leq C_l \frac{B_{f,N}^2 N^2 \log M}{M}\end{aligned}$$

Summing all the components gives

$$\begin{aligned}\|(\mathcal{K}_N - \mathcal{K}_{N,M})P_N g\|_{\mathcal{H}} &\leq \left(N \sum_{l=1}^N c_l^2 C_l \frac{B_{f,N}^2 N^2 \log M}{M} \right)^{1/2} \\ &\leq \sqrt{C_l \frac{B_{f,N}^2 N^3 \log M}{M}} \|g\|_{\mathcal{H}}\end{aligned}\quad (\text{B.7})$$

where we used Parseval's Identity $\|g\|_{\mathcal{H}}^2 = \sum_{l=1}^{\infty} c_l^2$. Summing the approximation error (B.1), the bias error (B.3), and the variance error (B.7) gives the total error bound (40).

C Elastic-net-regularized multi-step EDMD learning with Pruning

Algorithm 1 Elastic-net-regularized multi-step EDMD with pruning of nonlinear observables

Input: Dataset $\mathcal{D} = \{(x_{j,k}, x_{j,0}, u_{j,k-1})\} \forall j \in [1, M_m], \forall k \in [1, H]$, the initial library of nonlinear observables $\psi : \mathbb{R}^{n_x} \rightarrow \mathbb{R}^N$, regularization parameters $\beta \geq 0, \tau \geq 0$, the pruning parameter $\epsilon_E \geq 0$, the MPC prediction horizon length H .

1. Divide \mathcal{D} into H pieces: for $k = 1, \dots, H$

$$\mathcal{D}_k = \{(x_{j,k}, x_{j,0}, u_{j,0}, \dots, u_{j,k-1})\}_{j=1}^{M_m};$$
2. Prepare the matrix \mathbf{G} (59) by computing $\psi(x_{j,0})$;
3. **for** $k = 1, \dots, H$ (**in parallel**):
 - 3.1. Prepare the matrix \mathbf{H}_k (59);
 - 3.2. **for** $i = 1, \dots, n_x$ (**in parallel**):
 - 3.2.1. Prepare the vector h_k^i (60);
 - 3.2.2. $E_{k,i}, F_{k,i} \leftarrow$ the solution of (61);
 - 3.3. Get E_k by combining $E_{k,i}$: $E_k \leftarrow (\dots, E_{k,i}, \dots)^\top$;
 - 3.4. Get F_k by combining $F_{k,i}$: $F_k \leftarrow (\dots, F_{k,i}, \dots)^\top$;
4. Get E, F by combining E_k, F_k ;
5. The index set $L \leftarrow \emptyset$;
6. **for** $l = 1, \dots, N$: **if** $E_{l,:} \geq \epsilon_E$, **then set** $L \leftarrow L \cup \{l\}$; **end**
7. Pruning E, F : $E \leftarrow E_{L,:}, F \leftarrow F_{L,:}$;
8. Pruning the nonlinear observable ψ : $\psi \leftarrow \psi_L$;
9. $N \leftarrow \text{card}(L)$;
10. **end**.

Output: Multi-step Koopman predictor with E, F matrices, and nonlinear observables ψ .